



Multi-stage exhumation history of the West Kunlun orogen and the amalgamation of the Tibetan Plateau

Guangwei Li ^{a,b,*}, Mike Sandiford ^b, Aimin Fang ^c, Barry Kohn ^b, Dan Sandiford ^b, Bihong Fu ^d, Tongliang Zhang ^e, Yuanyuan Cao ^e, Fei Chen ^e

^a School of Earth Sciences and Engineering, Nanjing University, Nanjing, 210023, China

^b School of Earth Sciences, The University of Melbourne, 3010 Melbourne, Australia

^c Institute of Geology and Geophysics, Chinese Academy of Sciences, Beijing, 100029, China

^d Institute of Remote Sensing and Digital Earth, Chinese Academy of Sciences, Beijing, China

^e Xinjiang Institute of Engineering, 450016, Xinjiang, China



ARTICLE INFO

Article history:

Received 23 March 2019

Received in revised form 4 September 2019

Accepted 9 September 2019

Available online xxxx

Editor: A. Yin

Keywords:

exhumation

low temperature thermochronology

West Kunlun

Tibetan Plateau

ABSTRACT

The West Kunlun range, along the northwest margin of the Tibetan Plateau contains an important record of plateau formation and its northwards expansion. However, apart from the well-documented Miocene tectonism, its long-term history of exhumation/uplift remains enigmatic. Here we report an integrated low-temperature thermochronology study (apatite fission track and corresponding zircon (U-Th)/He) across a N-S transect through the West Kunlun range that reveals a prolonged low-temperature thermochronological record, characterized by a complex mosaic of thermal histories from the individual terrane elements during amalgamation to form the Tibetan Plateau. Our new data reveal two prominent cooling episodes during the Cretaceous and the Neogene, as well as several other more subdued and/or localized cooling episodes. Late Permo-Triassic cooling correlates with the accretion of the West Kunlun, Songpan-Ganzi and Tianshuihai terranes. Early Cretaceous cooling is considered as a response to collision between the Qiangtang and Lhasa terranes, while Late Cretaceous cooling relates to collision between the Karakorum terrane and Kohistan-Ladakh Arc. Partially preserved evidence for cooling in the Paleocene-Early Eocene and latest Oligocene-Miocene likely relates to the early stages of Indo-Asian collision. Our work confirms relatively low Neogene denudation rates of about 0.1–0.2 km/myr consistent with its arid, intraplate tectonic setting with deformation resulting from stress propagated via the surface plates and most likely sourced in the buoyancy of the plateau itself.

© 2019 Elsevier B.V. All rights reserved.

1. Introduction

The Cenozoic collision between the Indian and Asian plates resulted in the formation of the Tibetan Plateau and the Himalaya, as well as the rejuvenation of older orogenic belts such as the Longmenshan, East Kunlun-Qilianshan West Kunlun, and Tianshan mountain systems (e.g. Tapponnier et al., 2001; Yin, 2006; Fig. 1A). The formation of the plateau and related orogenic belts play an important role in the regional and global climatic system (e.g. Molnar et al., 2010). Considerable effort has focused on researching uplift of the plateau and geodynamic processes (e.g. Li et al., 2015; references therein), and the mechanisms that sustain the ongoing deformation. The mountain belts that bound the plateau

have been a particular research focus, although the level and style of activity is varied. The bounding systems vary considerably in terms of geomorphologic expression, fault style, slip rates, seismic expression and climate regimes. For example, the convergence rate across the Himalaya (~20–50 mm/yr; Zhang et al., 2004) is an order of magnitude higher than across the West Kunlun (<5 mm/yr) (Guilbaud et al., 2017; references therein) consistent with their respective plate boundary and intraplate settings. Of all the bounding systems, the West Kunlun remains the most poorly documented and enigmatic. The occurrence of deep earthquakes (~90 km) at near Moho levels in exceptionally thick crust beneath (Craig et al., 2012) highlight its unique importance to understanding the diversity of processes responsible for building the Tibetan Plateau.

Modern thermochronologic methods provide powerful tools enabling reconstruction of the cooling and exhumation history of both modern and ancient orogenic systems. For example, the apatite fission track (AFT) and zircon/apatite (U-Th)/He (ZHe/AHe) can record the time when rocks pass through their partial re-

* Corresponding author at: School of Earth Sciences and Engineering, Nanjing University, Nanjing, 210023, China.

E-mail address: guangweili@nju.edu.cn (G. Li).

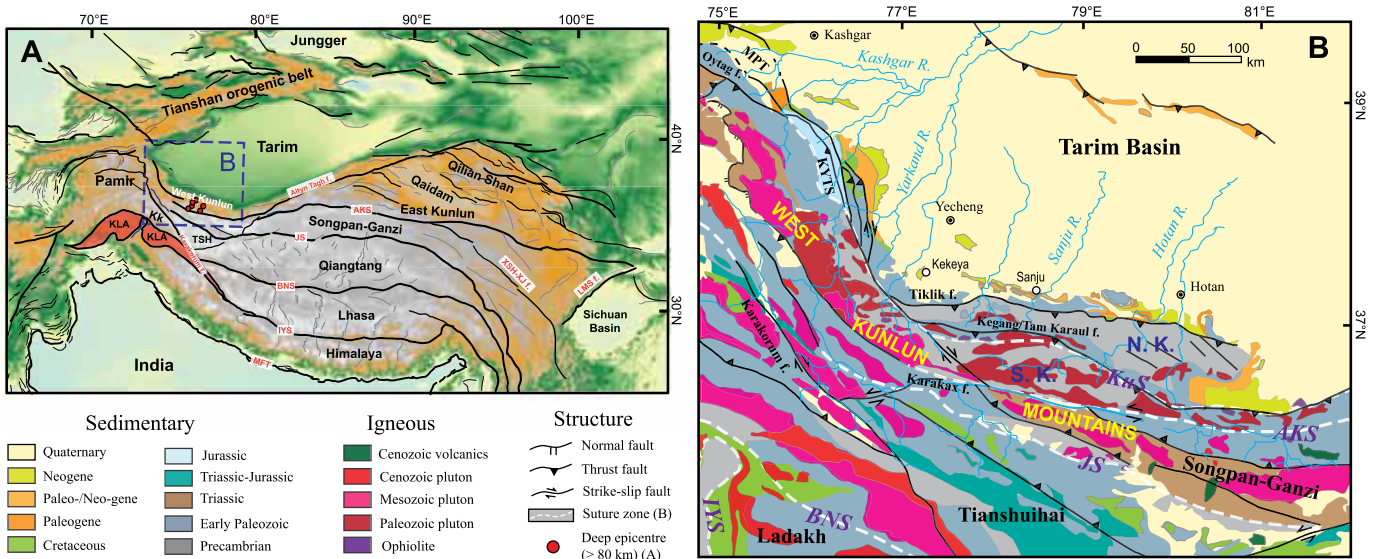


Fig. 1. A – Tectonic units of Tibetan Plateau and neighboring region. B – Simplified geological map of West Kunlun area (e.g. Wang et al., 2004). AKS = Animaqing-Kunlun suture, BNS = Bangong suture, IYS = Indus-Yarlung suture, JS = Jinsha suture, KuS = Kudi suture; KLF – Karakorum Fault; KF – Karakash Fault; LMS f. = Longmenshan fault, MFT = Main Front Thrust, MPT = Main Pamir Thrust, KYTS = Kashgar-Yecheng Transition system, XSH-XJ f. – Xianshuihe-Xiaojiang Fault. Kk = Karakoram terrane, KLA = Kohistan-Ladakh Arc, TSH = Tianshuhai, N.K. = Northern West Kunlun, S.K. = Southern West Kunlun. (For interpretation of the colors in the figure(s), the reader is referred to the web version of this article.)

tention/annealing zones (typically AHe: ~30–120 °C; AFT: ~60–110 °C; ZHe: ~130–200 °C; Guenthner et al., 2013; references therein). The results of thermochronological studies have been reported from most margins of the plateau, including the southern (e.g. Thiede and Ehlers, 2013; references therein), eastern (e.g. Wang et al., 2012; Tian et al., 2014) and northeastern (e.g. Clark et al., 2010; Qi et al., 2016; Liu et al., 2017) regions, as well as to the northwest from the Pamir area (e.g. Cao et al., 2013; references therein). By comparison, only a few scattered apatite fission track data have been reported from the West Kunlun (e.g. Wang et al., 2003; Sobel and Dumitru, 1997; Cao et al., 2014; Cheng et al., 2017). Several sedimentologic, structural geological and seismologic studies focused on the foreland basin record in the piedmont of the West Kunlun (e.g. Jiang and Li, 2014; Cao et al., 2015; references therein), provide indirect constraints on the exhumation/uplift history of the West Kunlun. Most of these studies focus on the post-Oligocene record, and show a widespread Neogene cooling/denudation event. Cao et al. (2015) reported detrital zircon fission track data from Miocene foreland deposits, suggesting a more complex older exhumation history for the West Kunlun orogen. While Cao et al. (2015) provides some new insights into an earlier stage of mountain building in the West Kunlun, the cooling/exhumation history of the region is yet to be thoroughly constrained.

Here, we report a suite of low-temperature thermochronological data including apatite fission track (AFT) and corresponding zircon (U-Th)/He (ZHe) data from basement rocks across the West Kunlun. Our data provide new constraints on the exhumation of this hitherto poorly understood part of the Tibetan region.

2. Geological background

2.1. Tectonic overview of Tibetan Plateau and surrounding region

The geological underpinnings of the modern Tibetan Plateau were formed by the amalgamation of several terranes within the Asian plate through Paleozoic to Cenozoic time. From south to north, the plateau has been separated into five distinct terranes: the Himalaya, Lhasa, Qiangtang, Songpan-Ganzi, Kunlun-Qaidam-Qilian terranes. Terrane boundaries are marked by major structures: Indus-Yarlung suture (IYS), Bangong-Nujiang suture (BNS),

Jingsha suture (JS) and Anymaqen-Kunlun suture (AKS), respectively (Fig. 1A; Yin, 2006). In the western plateau, the Shyok suture separates the Karakorum terrane (Kk) from the Kohistan-Ladakh Arc (KLA), and the IYS separates the Kohistan-Ladakh terrane from India (Rehman et al., 2011; Fig. 1A).

In the southern Tibetan Plateau, the Indus-Yarlung suture zone, which includes remnants of the Neo-Tethyan oceanic crust, separates the Himalaya (India) to the south and Lhasa terrane (Asia) to the north (e.g. Yin, 2006). The final closure of the Neo-Tethys ocean and collision between the Indian and Asian plates is generally regarded as having occurred between 65–50 Ma, although some authors have argued for considerably younger ages (e.g. Ding et al., 2005; Hu et al., 2016; references therein). The Lhasa and Qiangtang terranes are separated by the Bangong-Nujiang suture and based on the sedimentary record collision between them commenced during the Early-Middle Cretaceous (e.g. Kapp et al., 2007, and references therein). To the north, the Songpan-Ganzi terrane is thought to be underlain by oceanic lithosphere and overlain by Upper Triassic turbidites with intrusive magmatic rocks (e.g. Yin and Harrison, 2000). The Songpan-Ganzi terrane is considered to have experienced double subduction in the Late Triassic comprising a north directed system beneath the Kunlun arc along the Kunlun-Anyenaqen suture zone and a south directed system beneath the Qiangtang terrane along the Jinsha suture zone (Yin and Harrison, 2000).

The East Kunlun-Qaidam terrane consists of a composite batholith (e.g. Paleozoic arcs, Middle to Late Proterozoic metamorphic gneiss, schist and marble), unconformably overlain by latest Proterozoic-Ordovician strata (Yin and Harrison, 2000), which extends westward to the West Kunlun (Fig. 1). The Qilian Shan is truncated by the left-lateral strike-slip Altyn Tagh Fault to the north, which transfers a significant component of the convergence between India and Asia into eastward extrusion of the northern plateau. Based on low-temperature thermochronology data, the Qilian Shan grew outwards toward the foreland in Miocene, creating a series of NW dextral transpressional faults and associated crustal-scale ramp anticlines (e.g. Qi et al., 2016; Fig. 1A).

The Tarim Basin is a large rhomb-shaped geomorphic entity to the north of the Tibetan Plateau characterized by a long-lived record of sedimentation. It comprises a basement of Neoarchean

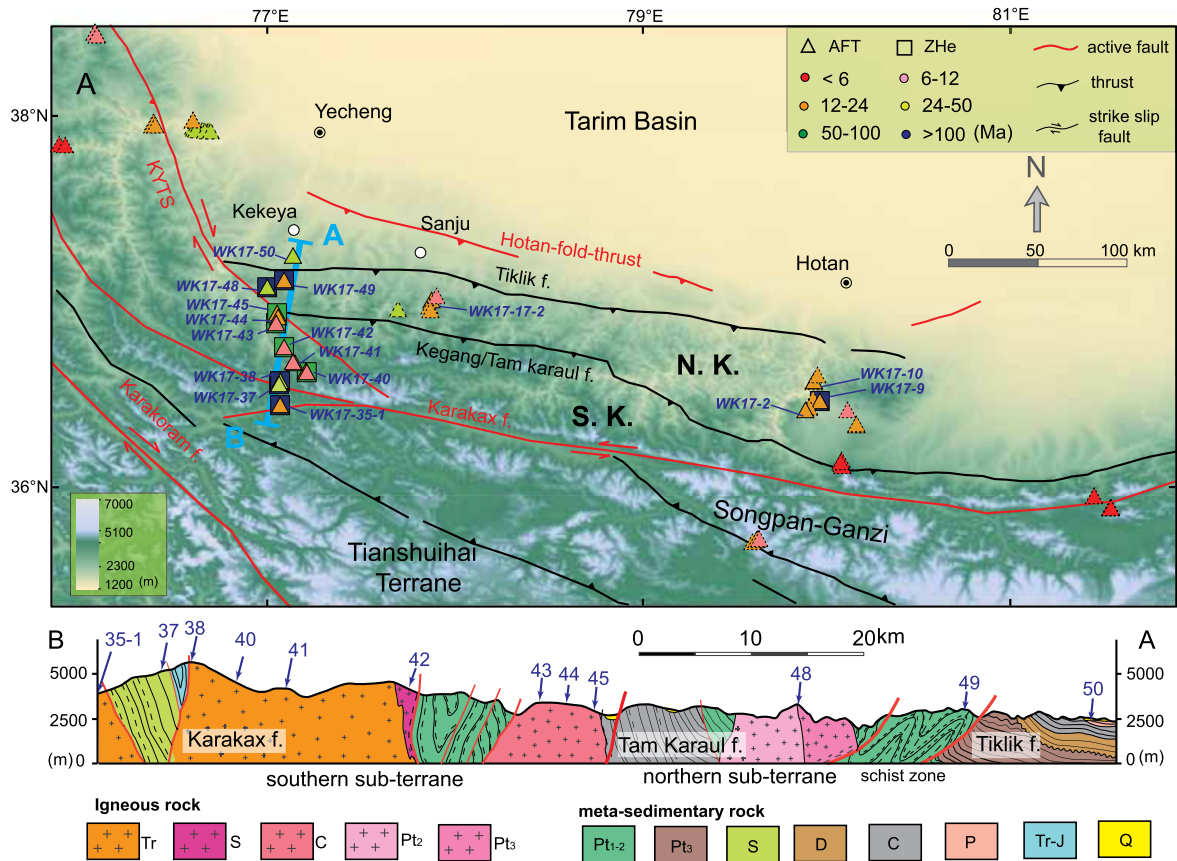


Fig. 2. DEM (SRTM 90 m) of the Tibetan Plateau with superimposed major structures, terranes and thermochronological data. Data from Sobel et al. (1997), Wang et al. (2003), Cheng et al. (2017) (marked as dashed triangle/rectangle) and this study (marked as solid triangle/rectangle). A-B marks the main sampling transect along 219 Highway (219 HW) in this study (modified after Wang et al., 2004).

to Paleoproterozoic metamorphic rocks, unconformably overlain by up to 15 km of Mesoproterozoic to Cenozoic marine to non-marine sediments (e.g. Zhao and Cawood, 2012; Fig. 1). The Tianshan orogenic belt bounds the Tarim Basin to the north (Fig. 1). As an important component of the Central Asian accretionary Orogenic Belt, it contains a record of the Palaeozoic collision between the Tarim, Yili and Junggar terranes (e.g. Xiao et al., 2015). The modern Tianshan mountain range reflects a succession of reactivation events during the Mesozoic and Cenozoic, the latest of which is associated with the India-Asia collision (e.g. De Grave et al., 2013; Dumitru et al., 2001).

2.2. Geology of West Kunlun Shan

The West Kunlun Range lies between the Tarim Basin (to the north), the Pamir salient (to the west) and the Tianshuaihai and Songpan-Ganzi terranes to the south, and is separated from them by the Kashgar-Yecheng transfer system (KYTS) and the Tiklik, Karakorum and the Karakax fault systems (e.g. Cowgill, 2001; Yin et al., 2002; Fig. 1B). Although the question of how sub-terrane of the Pamir salient relate to the better documented elements of the Tibetan Plateau further east remains somewhat controversial, the Tianshuaihai (TSH) terrane are generally accepted to correlate with the Qiangtang terrane (e.g. Robinson et al., 2015 and references therein).

The Tiklik fault bounding the north margin of the West Kunlun (Figs. 1B and 2) is a 300 km long, steeply south-dipping reverse fault that places garnet-bearing schist (Mitaz schist) over unmetamorphosed Paleozoic and Cenozoic sedimentary rocks to the north (e.g. Cowgill, 2001; Cao et al., 2014; Cheng et al., 2017 Figs. 1 and 2). It probably initiated in the Triassic (Cowgill, 2001)

and was reactivated in the Early Eocene (Yin et al., 2002) and/or Early Miocene (Wang et al., 2003; Jiang and Li, 2014). Oligocene-Early Miocene dextral transpression along the KYTS accommodated ~280 km northward translation of the Pamir relative to the more eastern terranes (e.g. Sobel and Dumitru, 1997; Cowgill, 2001; Cao et al., 2015). The Hotan fault is a blind thrust system that soles into basement of the Tarim along the piedmont of the West Kunlun, and above which lies an imbricated wedge of basement and cover strata (Jiang and Li, 2014; Cheng et al., 2017).

The West Kunlun is divided into northern and southern sub-terrane by the Kegang thrust along the Early Paleozoic Kudi suture zone (Mattern et al., 2000), which is also known as the Tam Karaul thrust (Cowgill, 2001; Fig. 1). The Tam Karaul fault places migmatitic gneisses against a schist belt to the north and is considered to correlate with the Main Pamir thrust (MPT) to the west (Yin et al., 2002; Cao et al., 2015, see Fig. 1B). The fault was active during the Cretaceous (Cowgill, 2001) and/or Eocene (Yin et al., 2002) and was reactivated in the Early Miocene (e.g. Wang et al., 2003; Jiang and Li, 2014). The northern sub-terrane mainly consists of Precambrian metamorphic basement, Paleozoic metasedimentary rocks, Ordovician-Silurian and Triassic arc-type plutons, and scattered ophiolites and ultramafic intrusions (Cowgill, 2001; Cao et al., 2015). Characterized by high topographic relief with peaks >6000 m, the southern sub-terrane consists of Proterozoic metamorphic rocks, intruded by late Paleozoic granitic batholith, elongated along the E-W strike of the terrane (Fig. 1B). The Songpan-Ganzi terrane consists of imbricated Paleozoic carbonates, Triassic flysch intruded by Triassic-Jurassic plutons, Jurassic-Cretaceous terrestrial sediments, and scattered

Late Miocene-Quaternary shoshonitic volcanics (e.g. Yin, 2006; Roger et al., 2011).

The active left-lateral Karakax fault separates the Songpan-Ganzi terrane to the south from the West Kunlun (Figs. 1B and 2). Local mélange complexes and fragments of serpentinites indicate Late Permian-Triassic suturing (the Mazar suture) (e.g. Mattern and Schneider, 2000), with further strike-slip faulting documented at ~120 Ma and ~25 Ma (Arnaud et al., 2003). The boundary between the Songpan-Ganzi and Tianshuihai terranes is marked by the Jinsha suture zone. Paleozoic strata in the Tianshuihai terrane has been proposed as an accretionary prism related to the northward subduction of Paleo-Tethys between the Tianshuihai and Karakorum terranes (Xiao et al., 2003). The Karakorum fault crosses the western Tibetan Plateau and locally slices the Karakorum and Tianshuihai terranes (Fig. 1).

The Karakax Fault forms part of the western extension of the Altyn Tagh Fault system and effectively separates the external part of the West Kunlun Range from the plateau interior. It converges westward towards the conjugate Karakorum Fault in a region characterized by some of the thickest crust in the Tibetan Plateau as well as unusual deep earthquakes (see Craig et al., 2012). With Quaternary slip rates estimated at 7.8 ± 1.6 mm/yr and a cumulative offset of around 80 km (Fu et al., 2006), its initiation likely extends back to ca. 10 Ma, at a similar time to some estimates for the inception of the most recent phase of right lateral motion on the Karakorum Fault (e.g. Lacassin et al., 2004). The combined ongoing slip on the Karakax and Karakorum faults accommodates several mm/yr of shortening by the east-southeast excision of the intervening Tibetan crustal wedge (to the south of the Karakax), with respect to the Kunlun.

3. Sampling and methods

In total, sixteen samples were collected from the West Kunlun in this study, comprising 14 granites, a schist, a Silurian sandstone (sample WK17-37) within the Tianshuihai terrane and a Permian sandstone (sample WK17-50) from the range front (Fig. 2). Twelve samples are from a N-S transect (219HW) across the West Kunlun at about 77°E (profile A-B, Fig. 2A). Four samples (WK17-2, -9, -10 and -17-2) were collected further east within the northern West Kunlun sub-terrane (Fig. 2). A summary of apatite fission track (AFT) and/or zircon U-Th/He (ZHe) data acquired from samples is presented in Tables 1 and 2.

Mineral separations and low temperature thermochronology were conducted at the School of Earth Sciences, University of Melbourne. For AFT analysis, data acquisition was carried out using a Zeiss Axio Imager M1m microscope with *Trackworks* and *Fast-Tracks* software developed by the Melbourne thermochronology group (Gleadow et al., 2015). Uranium concentrations of corresponding grains were determined using an Agilent 7700 LA-ICP-MS coupled with a New Wave UP-213 laser. Etch pit diameters (*Dpar*) were measured as the kinetic parameter for thermal history modeling. In addition, two mounts were made for all samples, one for age acquisition and another for the measurement of confined track lengths. To provide a more robust data set for inverse modeling, ^{252}Cf tracks were implanted into polished grains on the second mount to increase the number of confined track lengths available for measurement. Further details of the AFT and zircon (U-Th)/He analytical procedures follow descriptions in Gleadow et al. (2015) (see supporting information).

4. Results

4.1. AFT ages

AFT ages for all samples analyzed are significantly younger than their corresponding host stratigraphic/crystallization ages and

$P(\chi^2)$ values ranges from 11% to 44%, with a consistent dispersion value of zero (Table 1), which suggests that all these samples have all been thermally reset with respect to the AFT system. The twelve samples along the 219HW transect all yield Cenozoic AFT ages (<40 Ma), with nine yielding Miocene ages between ~21-7 Ma (Table 1). Samples WK17-38 and -48, from local elevation highs ('Mazha Daban' –4969 m and 'Kudi Daban' –3150 m) yield late Eocene AFT ages of 35.5 ± 3.3 and 38.5 ± 2.5 Ma, respectively, as does sample WK17-50 in the footwall of the Tiklik fault (>5 km from the fault plane) with a late Eocene AFT age of 35.2 ± 5.8 Ma (Fig. 3 and Table 1). All samples yield mean confined track length values, ranging from 12.9–13.9 μm (non-projected). Sample WK17-48 yields the oldest AFT age and shortest mean track length value of $12.9 \pm 1.7 \mu\text{m}$ (Table 1), while sample WK17-38 shows a bimodal track length distribution with a relatively long mean track length value of $13.3 \pm 1.5 \mu\text{m}$ (Fig. S1).

Four other samples from northeastern West Kunlun (Fig. 2) all yield Miocene AFT ages ranging between 9.6 ± 0.5 and 14.9 ± 1.1 Ma, with relatively long mean track lengths ranging between 13.0 ± 2.2 and $13.8 \pm 1.4 \mu\text{m}$, similar to those from the 219 HW transect (Table 1). These four ages are in accord with previously published AFT data from the same general area (e.g. Wang et al., 2003; Cheng et al., 2017).

4.2. ZHe ages

ZHe data from ten samples are presented in Table 2 (see Fig. 2). Nine of these generally yield reproducible pre-Cenozoic ages (at \pm the 2σ level), with single aliquot ages ranging from 74 to 266 Ma. Sample WK-40 yielded a weighted mean age of 56.6 ± 3.5 Ma (Table 2). Several grains with seemingly anomalously young ages were excluded from the weighted mean age calculation because of their relatively high eU content (e.g. grains WK17-40c, WK17-42c, WK17-45c, WK17-37b; Table 2). eU (ppm) can be viewed as a proxy for α -radiation damage (Shuster et al., 2006) and higher values are considered to be a major factor linked to increased He diffusivity (e.g. Guenthner et al., 2013). In this respect, it is noted that all grains in sample WK17-09 have relatively high eU content (1294.2–1624.5 ppm), and so the apparent ages (92.6–137 Ma) are probably younger than the actual timing of passage through the nominal closure temperature zone because of the high eU effect (Table 2). The nine samples along the 219HW transect are characterized by relatively young ZHe ages (Late Cretaceous-Eocene) within the southern Kunlun sub-terrane with older ages (Early Cretaceous- Permian/Triassic) distributed both to the south and north (Fig. 3 and Table 2). Sample WK17-09 from the eastern part of the northern Kunlun sub-terrane yields an Early Cretaceous age (Table 2), consistent with ages from samples in the northern Kunlun along the main transect. The older ages of samples WK17-38 and WK17-49 (229 ± 17 and 261 ± 22 Ma) suggest that they may have experienced a longer time with the zircon He partial thermal retention zone and resided at a shallower crustal level compared to other samples studied.

Although some samples show a locally positive age-elevation correlation, such as the southernmost samples WK17-35-1, WK17-37 and WK17-38 and samples WK17-48 and WK17-49 (Fig. 3), most show a slight variation. The similarly old AFT ages for samples WK17-38, WK17-48, and WK17-50 suggest that they probably cooled through the ZHe partial retention zone at the same time (Fig. 3).

5. Thermal history modeling

5.1. Modeling approach

We have reconstructed the thermal histories for twelve samples employing inverse modeling using the HeFTy software (Ketcham,

Table 1
Apatite fission track data for West Kunlun Range.

Sample No.	Sample information				Age results							Track length and Dpar results			Mean Dpar (range) (μm)	
	Group	Lithology	Locality ($^{\circ}\text{E} / ^{\circ}\text{N}$)	Elevation (m)	No. of grains (n)	No. (n)	Spontaneous tracks Density (10^5 cm^{-2})	Pooled ^a ^{238}U (ppm)	Pooled ^b age (Ma \pm 1SD)	P(χ^2) ^c (%)	Dispersion (%)	Central age ^d (Ma \pm 1SD)	^e Non-projected Mean ($\mu\text{m} \pm 1\text{SD}$)	Projected ⁶ Mean ($\mu\text{m} \pm 1\text{SD}$)	No. (n)	
219 HW Transect																
WK17-35-1	W	granite	77.004/36.446	3781	28	297	2.664	33.7	15.9 \pm 1.0	42	0	16.6 \pm 1.0	13.3 \pm 1.5	14.3 \pm 1.0	132	1.7 (1.5-2.1)
WK17-37	W	schist	77.000/36.561	4789	11	20	1.649	11.37	28.4 \pm 3.2	29	0	29.7 \pm 6.9				1.4 (1.2-1.5)
WK17-38	W	granite	77.003/36.579	4969	17	62	1.418	9.53	35.5 \pm 3.3	30	0	37.7 \pm 5.0	13.3 \pm 1.5	14.0 \pm 1.2	15	2.19 (1.4-2.8)
WK17-40	W	granite	77.147/36.627	4001	26	98	1.325	23.5	11.3 \pm 1.5	40	0	12.5 \pm 1.3	13.6 \pm 1.8	14.6 \pm 1.2	93	1.6 (1.5-1.9)
WK17-41	W	granite	77.083/36.674	3606	21	112	1.709	18.2	20.5 \pm 2.1	44	0	22.3 \pm 2.2	13.2 \pm 1.6	14.2 \pm 1.2	129	1.6 (1.4-1.8)
WK17-42	W	granite	77.026/36.763	3170	25	206	1.572	45.5	6.7 \pm 0.6	29	0	7.1 \pm 0.5	13.7 \pm 1.4	14.5 \pm 1.0	139	1.6 (1.5-1.7)
WK17-43	W	granite	76.982/36.895	2952	27	115	7.661	14.8	11.5 \pm 2.2	37	0	12.1 \pm 1.2	13.9 \pm 1.3	14.7 \pm 1.0	80	1.5 (1.4-1.6)
WK17-44	W	granite	76.993/36.928	2802	24	256	1.552	20.2	16.3 \pm 1.4	11	0	16.8 \pm 1.1	13.5 \pm 1.3	14.5 \pm 1.0	129	1.5 (1.3-1.7)
WK17-45	W	granite	76.985/36.949	2674	25	130	1.314	20.4	12.5 \pm 1.2	43	0	13.7 \pm 1.3	13.4 \pm 1.3	14.3 \pm 1.0	14	1.5 (1.3-1.7)
WK17-48	NW	granite	76.935/37.090	3150	27	360	1.970	9.48	38.5 \pm 2.5	32	0	39.9 \pm 2.3	12.9 \pm 1.7	14.0 \pm 1.3	146	1.6 (1.4-1.8)
WK17-49	NW	sandstone	77.024/37.128	2549	27	91	1.638	25.1	13.1 \pm 1.3	33	0	14.0 \pm 1.5	-	-		2.1 (1.3-3.3)
WK17-50	NW	sandstone	77.074/37.213	2342	10	145	3.872	19.0	35.2 \pm 5.8	14.4	0	38.4 \pm 4.5	-	-		1.5 (1.3-1.7)
Northern W. Kunlun – further east																
WK17-2	E	granite	80.113/36.419	2555	18	98	0.710	13.2	11.3 \pm 1.6	21	0	12.2 \pm 1.3				1.4 (1.2-1.6)
WK17-9	E	granite	79.959/36.473	2159	27	244	1.017	13.7	14.9 \pm 1.1	39	0	15.6 \pm 1.0	13.0 \pm 2.2	14.0 \pm 1.6	131	1.5 (1.4-1.8)
WK17-10	E	granite	79.923/36.480	2082	29	132	0.839	11.8	14.6 \pm 1.3	50	0	15.4 \pm 1.4	13.5 \pm 1.7	14.4 \pm 1.2	88	1.5 (1.4-1.9)
WK17-17-2	E	granite	77.861/37.042	2612	26	361	2.480	50.3	9.6 \pm 0.5	70	0	9.6 \pm 0.6	13.8 \pm 1.4	14.6 \pm 1.1	125	1.6 (1.5-1.8)

^a Pooled uranium content of all grains measured by LA-ICP-MS.

^b Pooled AFT age of all grains.

^c P-value of χ^2 for (n-1) degrees of freedom.

^d Lengths measured after ^{252}Cf irradiation.

^e c-axis projected mean track length (after Ketcham et al., 2007).

Table 2
Zircon (U-Th)/He data for West Kunlun Range.

Sample No.	${}^4\text{He}$ (ncc)	Mass (mg)	Mean ^a F_T	U (ppm)	Th (ppm)	Th/U	[eU] ^b (ppm)	Corrected age (Ma)	Error $\pm 1\sigma$	Grain length (μm)	Grain half width (μm)	Crystal ^c morphology
WK17-09a	188.404	0.0103	0.79	1492.3	510.7	0.34	1612.3	92.6	5.7	335.1	59.9	2T
WK17-09b	216.014	0.0098	0.79	1508.1	495.2	0.33	1624.5	110.2	6.8	309.1	61.0	2T
WK17-09c	282.160	0.0129	0.80	1183.2	472.2	0.40	1294.2	137.3	8.5	359.4	64.8	2T
WK17-35-1a	50.502	0.0106	0.83	353.8	165.3	0.47	392.6	98.9	6.1	217.5	64.1	2T
WK17-35-1b	46.716	0.0084	0.81	389.9	202.5	0.52	437.5	103.8	6.4	212.8	57.5	2T
WK17-35-1c	57.497	0.0089	0.80	381.5	189.9	0.50	426.2	124.0	7.7	245.1	55.7	2T
WK17-37a	116.561	0.0252	0.86	192.7	68.3	0.35	208.7	179.0	11.1	356.5	78.3	2T
WK17-37b	166.190	0.0126	0.84	695.3	342.6	0.49	775.9	138.1	8.6	248.4	65.3	2T
WK17-37c	54.263	0.0071	0.78	314.8	145.9	0.46	349.1	176.3	10.9	221.6	52.4	2T
WK17-38a	88.880	0.0112	0.82	209.9	146.3	0.70	244.3	260.1	16.1	257.4	61.0	2T
WK17-38b	88.855	0.0073	0.79	413.4	335.1	0.81	492.1	200.0	12.4	237.0	51.7	2T
WK17-38c	88.720	0.0067	0.78	416.1	67.7	0.16	432.0	245.2	15.2	238.3	49.7	2T
WK17-40a	35.353	0.0 105	0.81	414.5	245.4	0.59	472.2	58.4	3.6	269.4	58.2	2T
WK17-40b	45.552	0.0124	0.83	494.5	225.0	0.45	547.3	54.8	3.4	269.8	62.8	2T
WK17-40c	31.135	0.0052	0.76	947.5	420.6	0.44	1046.4	46.6	2.9	209.7	46.4	2T
WK17-42a	104.803	0.0144	0.82	711.6	216.5	0.30	762.4	78.2	4.8	330.0	62.4	2T
WK17-42b	100.342	0.0170	0.83	541.8	200.7	0.37	589.0	82.0	5.1	340.6	66.5	2T
WK17-42c	104.668	0.0093	0.80	1764.0	199.8	0.11	1810.9	50.7	3.1	257.5	56.1	2T
WK17-43a	32.515	0.0065	0.79	358.6	274.6	0.77	423.1	96.7	6.0	206.8	51.5	2T
WK17-43b	13.992	0.0053	0.76	246.3	178.9	0.73	288.4	74.1	4.6	216.3	46.4	2T
WK17-43c	22.354	0.0094	0.79	248.8	131.7	0.53	279.7	69.8	4.3	287.4	54.1	2T
WK17-45a	22.068	0.0044	0.76	463.1	422.3	0.91	562.3	73.6	4.6	168.8	54.8	2T
WK17-45b	53.157	0.0059	0.77	559.2	503.5	0.90	677.6	109.0	6.8	210.9	43.5	2T
WK17-45c	22.192	0.0048	0.75	608.8	1691.2	2.78	1006.2	37.6	2.3	177.7	47.6	2T
WK17-48a	45.411	0.0109	0.82	334.9	67.4	0.20	350.8	96.5	6.0	275.6	58.8	2T
WK17-48b	39.236	0.0088	0.78	272.4	101.3	0.37	296.3	123.0	7.6	312.2	51.0	2T
WK17-48c	26.120	0.0078	0.78	227.3	107.2	0.47	252.5	107.5	6.7	267.2	51.2	2T
WK17-49a	88.285	0.0078	0.80	284.0	240.4	0.85	340.5	266.6	16.5	215.7	55.2	2T
WK17-49b	24.253	0.0057	0.77	105.4	120.9	1.15	133.8	255.1	15.8	192.5	50.0	2T

Note: Grains marked in italics indicate that their relatively younger intra-grain ages can be directly attributed to their high eU values (Guenthner et al., 2013).

^a F_T is the ejection correction after Farley et al. (1996).

^b Effective uranium content eU = [U ppm + 0.235 * Th ppm].

^c Grain morphology – 2T = 2 crystal terminations.

2007). AFT data was modeled using the multi-kinetic annealing model of Ketcham et al. (2007), with D_{par} as a kinetic parameter. ZHe data were modeled using the helium diffusion model of Guenthner et al. (2013). Two initial constraints were applied for thermal history modeling: (1) an initial temperature-time constraint was set at 240–120 °C (except for the sample WK17-17-2 with 140–50 °C due to only AFT data used) at a time span older than the corresponding weighted mean ZHe age; (2) a temperature of 15 ± 5 °C was assumed for the mean present surface.

Samples WK17-09, WK17-35-1, WK17-38, WK17-40, WK17-42, WK17-43, WK17-WK17-45 and WK17-48 were modeled using combined ZHe and AFT data; samples WK17-10, WK17-41 and WK17-44 were modeled with AFT data using constraints from ZHe ages from nearby samples WK17-09, WK17-42 and WK17-45, respectively. Sample WK17-17-2 was modeled only based on AFT data (Fig. S1 and S2 in the Supporting Information). For modeling, c-axis projected lengths (many enhanced by ${}^{252}\text{Cf}$ irradiations) were used, with models run so as to obtain 100 ‘Good-Fit’ paths (merit value: 0.5).

5.2. Thermal history modeling results

Thermal history models of the low temperature thermochronology data reveal multiple cooling episodes within the West Kunlun orogen (Fig. 4; Supporting Information Figs. S1–S2). Along the 219HW transect, sample WK17-38 with the highest elevation (Kudi Daban) shows the oldest cooling episode during Permian and Triassic time, followed by prolonged quiescence until a subsequent

cooling phase commencing in the Eocene (Figs. 4 and S1). Samples WK17-35-1 and WK17-48 show an Early Cretaceous cooling episode, while samples WK17-42, WK17-43, WK17-44 and WK17-45 also indicate a Late Cretaceous cooling episode. Samples WK17-40 and WK17-41 record a late Cretaceous-Early Eocene cooling episode. It is worth noting that two samples WK17-38 and WK17-48 from mountain passes (Kudi and Maza Daban), near the Karakax and Tiklik faults respectively (Fig. 3), indicate subsequent cooling event in the Eocene (~45 Ma). A pronounced Miocene cooling episode is recorded by all samples albeit with the suggestion of some variation in the timing of onset (Fig. 4). Further, the late Permian ZHe age for sample WK17-49 probably also reflects some cooling at this time, although the absence of AFT length data preclude the construction of the thermal history for this sample (Tables 1, 2; Fig. 4).

Samples WK17-9 and WK17-10 from further east show consistent Early Cretaceous and Miocene cooling episodes. Sample WK17-17-2 only shows Middle Miocene cooling, followed by slow cooling from the Late Miocene (see Fig. 4 and Supporting Information). This sample did not contain zircon, therefore the modeling is based solely on AFT data.

Cooling rates calculated from thermal histories derived by HeFTy show a complex spatial and temporal variation pattern (Fig. 5). Most samples (especially from the Karakax fault to the north) experienced relatively high cooling rates (>5 °C/Ma) during the Cretaceous and again during the Miocene with significantly lower rates (<1 °C/Ma) during Paleocene-Oligocene time. The exceptions are samples WK17-40 and WK17-41 which experienced

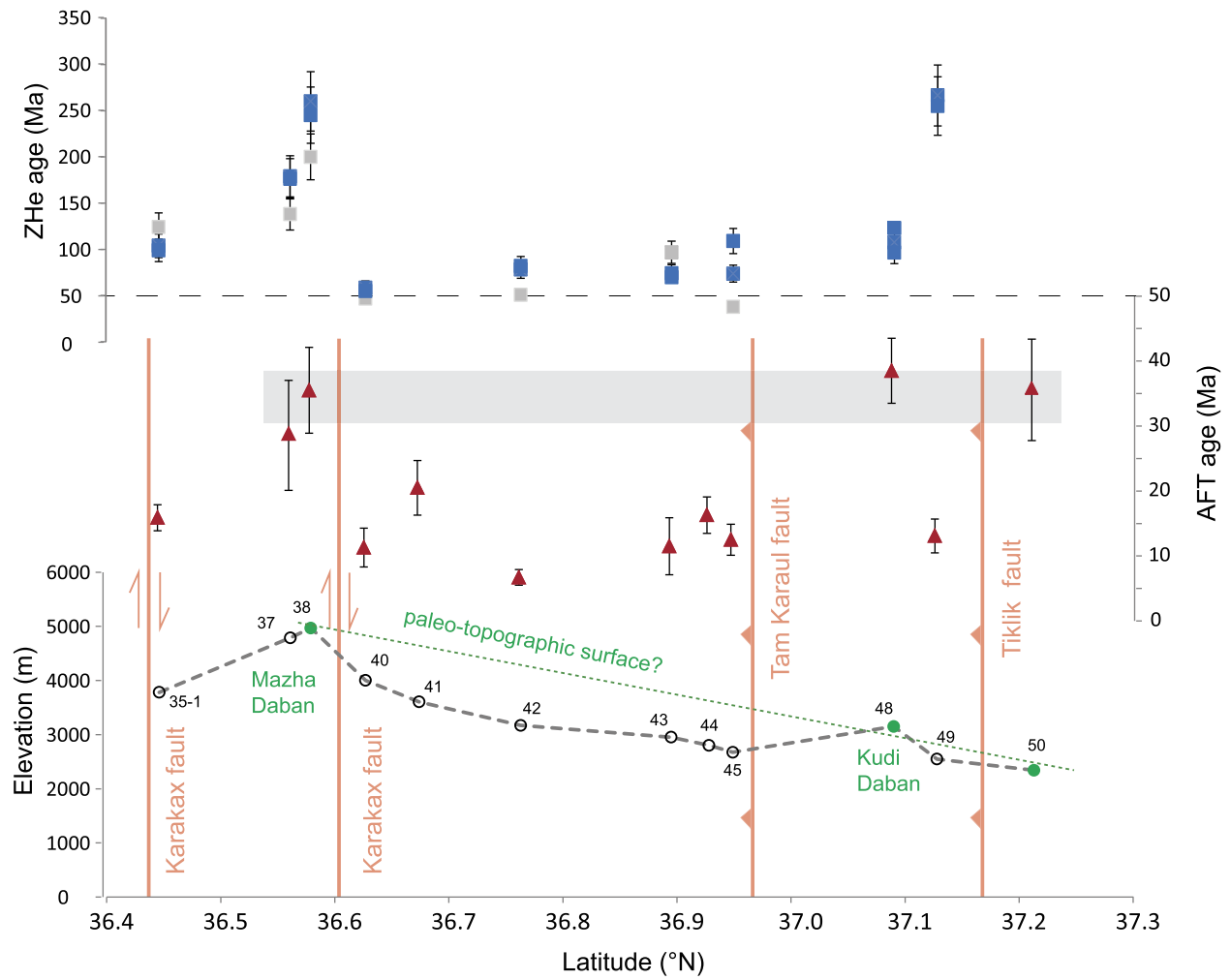


Fig. 3. Spatial pattern of apatite fission track and ZHe data (with 2σ) along the 219 HW transect in the West Kunlun. 35-1: sample WK17-35-1. For ZHe data, individual aliquot ages (see Table 2) of each sample are plotted. The grey square represents the aliquot ages excluded because of high eU effect.

Paleocene cooling rates $>5^{\circ}\text{C}/\text{Ma}$, and WK17-38 and WK17-49 which experienced cooling at rates of $\sim 3\text{--}4^{\circ}\text{C}/\text{Ma}$.

5.3. Age-elevation relationships

In eroding landscapes in which all samples have passed through the partial annealing zone (PAZ), AFT age distributions are expected to correlate with elevations, with the slope of the correlation dependent on the characteristic erosion rate. In reality, the nature of the correlation is sensitive to the spatio-temporal character of erosion and topography, and particularly, the history of fault motion, and the variation in the way individual samples preserve the cooling record (e.g. Fitzgerald and Malusà, 2019).

The elevation-age relations for the West Kunlun AFT results are summarized in Fig. 8. For this analysis we subdivide the analysis into three groups (see Table 1); the E-group from the Tikklik massif, and the NW- and W-groups, including samples along the main transect at 77°E to the north and south of the Tam Karaul fault, respectively. The E- and NW-groups show only a limited elevation range, with a wide range of ages in the NW-group indicative of juxtaposition of fault blocks with rather different closure histories in the foreland part of the orogenic wedge. In contrast the array of W-group AFT ages shows a moderate correlation ($R^2 = 0.64$) over an elevation range of 2.3 km yielding a slope of $0.073 \pm 0.021 \text{ km/myr}$ (Fig. 6).

To assess the significance of this array, we compare it with the expectations of a steady state erosion. Thermal advection associ-

ated with erosion tends to compress isotherms against the upper (cooling) surface (e.g., Fitzgerald and Malusà, 2019) and so for a given topography, both the mean AFT age, as well as the spread in ages, will decline with increasing erosion rate (Fig. 7). In the steady state limit, for which topography and erosion rate are both spatially and temporally invariant, this effect is dependent on the spectral character of the topography, the reference geothermal gradient and the bulk thermal properties of the eroding rock mass. This effect can be quantified using the semi-analytical methods developed by Mancktelow and Grasemann (1997) and Wei and Zhou (2009) (see supporting information) and inverted for the duration of exhumation from a given depth or thermal condition across the prescribed topography. Fig. 9 summarizes the expected distribution of exhumation duration (in myr) from 100°C for erosion rates between 0.065 and 0.3 km/myr in the steady state limit, for a topography derived from the Shuttle Radar Topographic Mission (STRM) along an orogen parallel profile centered on the locus of the W-group sample set. Here the topography has ~ 3.6 km relief, varying between 2.6 and 6.2 km. We assume a reference geothermal gradient of $35^{\circ}\text{C}/\text{km}$, but find our results are relatively robust to variations in gradient of $\pm 15^{\circ}\text{C}/\text{km}$ spanning the likely conditions, because under these conditions the topographic relief provides the dominant control on thermal structure of the shallow crust.

AFT track retention occurs across a range of temperatures depending principally on rates of cooling and apatite chemistry, and

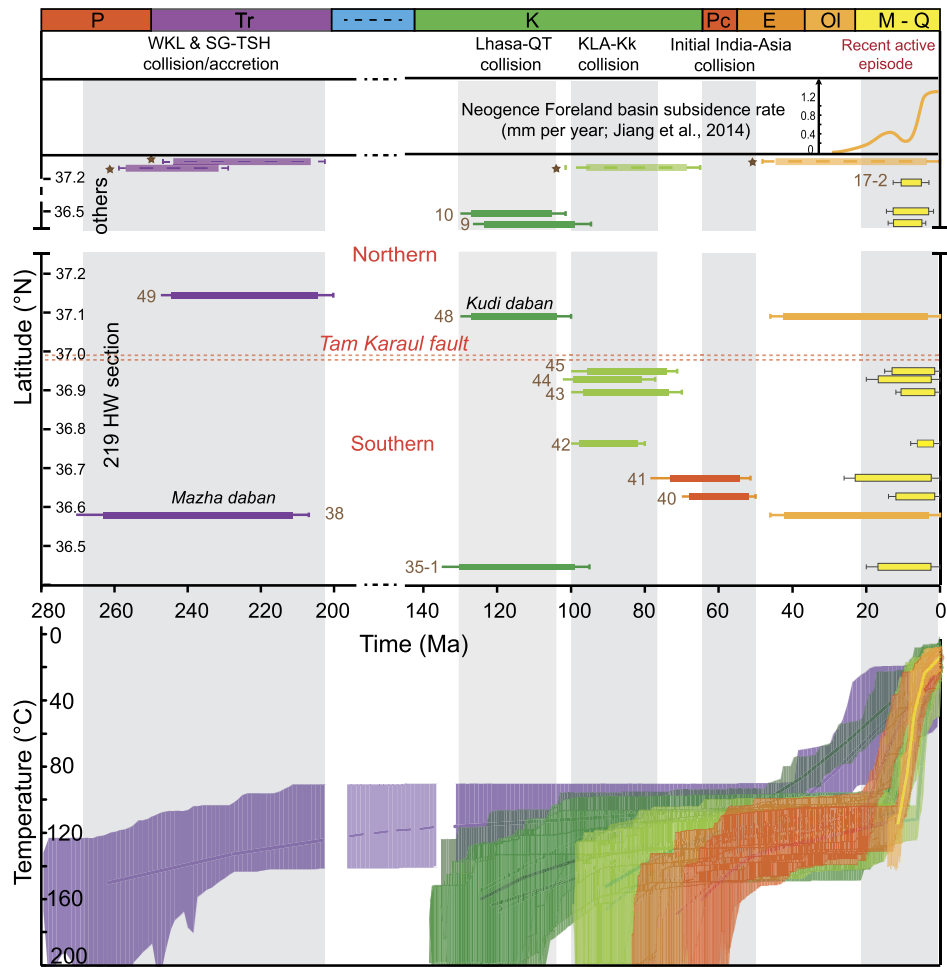


Fig. 4. Cooling history of the West Kunlun and geological events recorded in different terranes of the Tibetan Plateau. Upper panel: fast cooling episodes of West Kunlun, shown by horizontal bars, based on the thermal history modeling below. Those episode bars marked with asterisk cited from Cowgill (2001); the sample number e.g. '40' = 'WK17-40'. Lower panel: Cooling histories of ten samples based on thermal history modeling of ZHe and AFT data. Envelopes encompass all 'Good Fit' models obtained for these samples using a merit value of 0.5, while thick lines represent best-fit models for analytical data (Ketcham et al., 2007). Details of modeling results are shown in supporting information. P – Permian; Tr – Triassic; K – Cretaceous; Pc – Paleocene; E – Eocene; OI – Oligocene; M-Q – Miocene-Quaternary; other abbreviations for Fig. 1. Geologic events compiled from Yin and Harrison (2000; QT-SG collision); Yin (2006; Lhasa-QT collision); Rehman et al. (2011; KLA-Kk collision); Hu et al. (2016; Initial India-Asia collision).

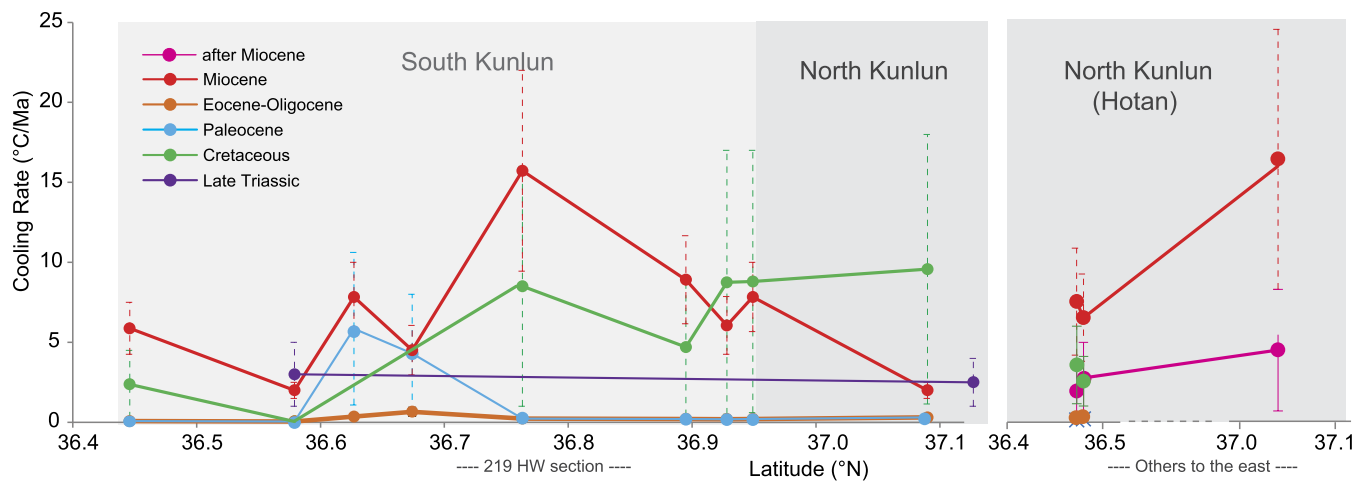


Fig. 5. Mesozoic-Miocene cooling rates of West Kunlun calculated from thermal history HeFTy modeling results.

cannot be reconciled with a single isotherm. However, for comparative purposes, we choose a nominal value of 100 °C as being representative for AFT closure for our sample set because they preserve relatively long track lengths indicative of relatively short

transit through the PAZ. In particular, our thermal history modeling described above shows all modeled W-group samples have been cooled from temperatures above about 100 °C since the onset of mid-Cainozoic cooling. As summarized in Fig. 8, the comparison

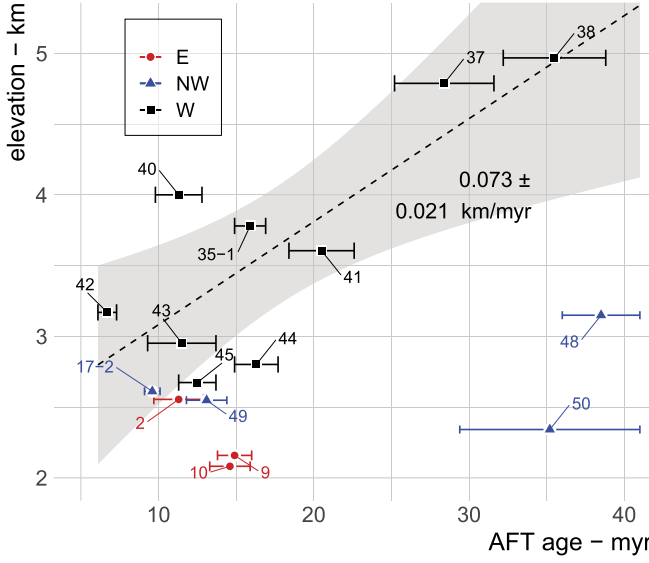


Fig. 6. Summary of elevation – AFT age distribution for West Kunlun samples by subgroups E, NW and W (see Table 1). The best fit for the W-group, which comprises those samples between the Tam Karaul and Karakax Faults, shows a moderate correlation ($R^2 = 0.64$) with slope 0.073 ± 0.021 km/myr.

of the observed data with the synthetic results suggests that the peak in AFT ages peak at ~ 15 Ma, is broadly consistent with time averaged erosion rates of about ~ 0.2 km/myr.

In detail, our observed data defines an elevation-age array that is shallower than expected for a steady state conditions at erosion rates greater than ~ 0.15 km/myr. It is clear therefore, steady state conditions do not apply (Fig. 8). This discrepancy in slopes can be interpreted in several ways. For example, the highest sample from ~ 5 km elevation (WK17-38) may have been exhumed from within the PAZ during the relevant phase of cooling. Alternatively, such an array can be interpreted in terms of either: 1) a spatial distribution of erosion rates that had contributed to growth in topographic relief (i.e., valleys are incising faster than interfluves are eroding), or

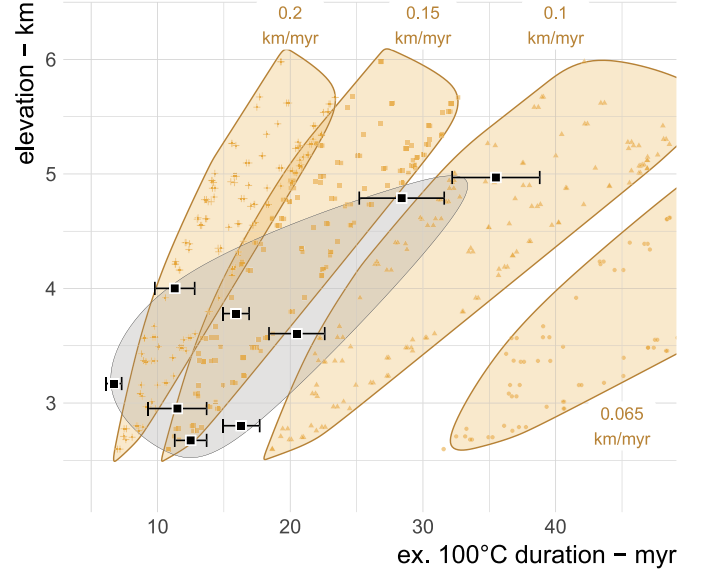


Fig. 8. Plot (in orange) of synthetic elevation versus age/duration using steady state erosion model for a representative topographic profile with 3.6 km relief (between 2.6 and 6.2 km ASL). The duration is the time taken to exhume rocks from the depth of the 100°C isotherm to surface exposure, assuming steady state thermal conditions and temporally and spatially invariant erosion rates of 0.065, 0.1, 0.15, and 0.2 km/myr. Note that the observed data from the W-group (black) defines an array that is shallower than the synthetic data for erosion rates greater than about 0.15 km/myr, suggesting that the relief in this part of the West Kunlun is still growing, or that the erosion rate has, on average, increased between the early and late Neogene (see text for further discussion).

2) temporal changes that have increased erosion rates over since about 15 Ma.

The fact that samples in the W-group including WK17-38 all have along AFT length distributions implies that they all passed through the PAZ relatively quickly. Consequently, we prefer to interpret the observed apparent shallow slope of the age-elevation distribution in terms of either a growth in relief and/or systematic changes in erosion rate over time. While we have not attempted to quantify these effects using numerical methods, assuming that the

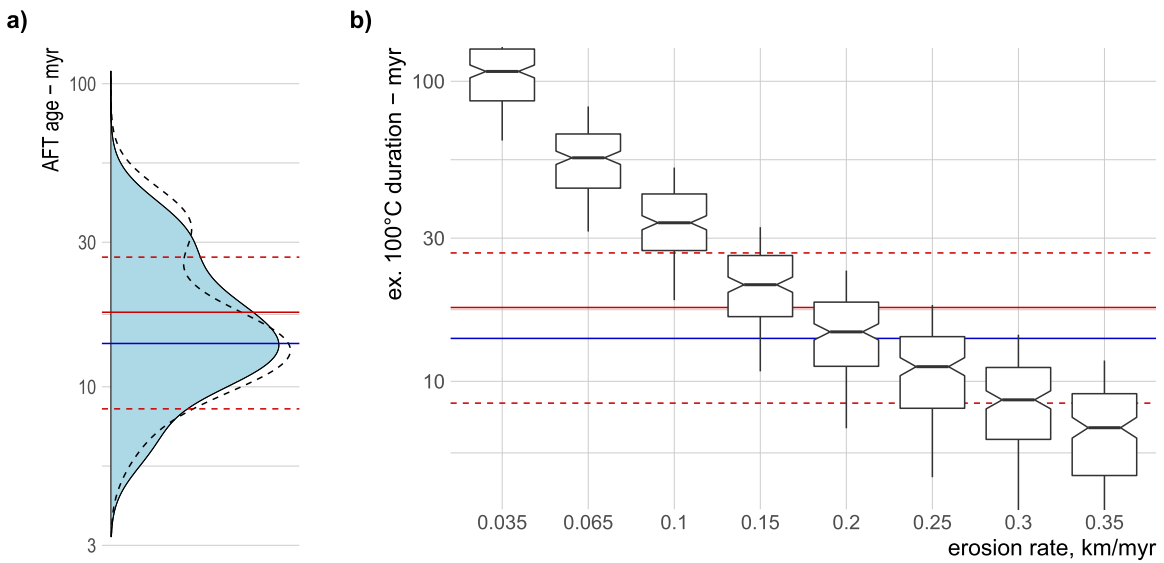


Fig. 7. Summary of elevation – AFT age distribution modeling. A) Dashed black line – kernel density distribution of AFT ages for all samples the West Kunlun. Solid black line with blue fill – kernel density distribution from the W-group, comprising samples along between the Tam Karaul Fault and Karakax Fault (see Table 1). Red line – mean of the W group. Red dashed lines – mean ± 1 standard deviation. Blue line – peak of the kernel density estimate for W-group. B) Durations (in myr) for exhumation from depths corresponding to the 100°C isotherm to the surface a characteristic topography derived from the modern West Kunlun, as a function of erosion rate assuming steady state conditions using the analytical solution of Mancktelow and Grasemann (1997 – see supporting information for details). Assumed initial geotherm $35^\circ\text{C}/\text{km}$, lapse rate $-4.5^\circ\text{C}/\text{km}$, characteristic surface temperature of 12°C at 1280 m ASL. Note logarithmic (base 10) age-scaling.

rate of relief production scales with the ratio of synthetic to observed age-elevation array slopes, we suggest that average erosion rates may vary in range from about 0.2 to 0.1 km/myr for valleys and interfluves, respectively, or erosion rates have doubled from about 0.1 to 0.2 km/myr between the early and late Neogene.

6. Discussion

Our new thermochronological data from the West Kunlun reveal a multi-stage cooling/exhumation history commencing in the early Mesozoic (Late Permian-Triassic) and terminating in a widespread Miocene cooling event (Figs. 3 and 4). In the following, we discuss the implications of these cooling episodes for the amalgamation of the Tibetan Plateau as well as the Neogene denudation of the West Kunlun.

The thermochronological record of the Kunlun reveals a cooling history showing: 1) a Late Permian-Triassic and Early Cretaceous relatively rapid cooling followed by a Late Cretaceous (~110–70 Ma) cooling in both the northern and southern Kunlun sub-terrane; 2) a Late Cretaceous to Early Eocene (~70–50 Ma) cooling in the southern sub-terrane; and 3) a widespread Miocene cooling across the entire West Kunlun (Fig. 4). These results are generally consistent with the detrital zircon fission track ages from the foreland basin in the West Kunlun piedmont (in the Kekeya and Sanjiu areas; Fig. 1B) reported by Cao et al. (2015) which show age-peaks at ~267–201, ~131–103, ~58–40, and ~23–7 Ma, as well as with MDD modeling of K-feldspar ^{40}Ar - ^{39}Ar data within the hanging wall of the Tiklik fault (Cowgill, 2001). The cooling rate patterns based on our HeFTy good-fit path envelopes highlight two main cooling episodes during the Cretaceous and Miocene, separated by a prolonged period of relative quiescence (Fig. 5). Below we provide context for understanding this complex cooling history.

The oldest record of cooling (Late Permo-Triassic) is recognized in the southernmost (sample WK17-38), and northernmost of the West Kunlun (e.g. sample WK17-49, and K-feldspar ^{40}Ar - ^{39}Ar data reported by Cowgill, 2001), and correlates with the inferred collision or accretionary history of the Songpan-Ganzi and Tianshuihai terranes at that time (e.g. Mattern and Schneider, 2000). These terranes comprise a series of intrusive magmatic belts, volcanic arcs and sedimentary wedges that were accreted during closure of the Paleo-Tethys Ocean along the Jinsha suture, and collision between the peri-Gondwanan/Cimmerian fragment of Qiangtang with southern Asia (specifically the Songpan-Ganzi terrane) in the Triassic (Yin and Harrison, 2000).

Exhumation associated with these events is preserved in the thermochronological record across the northern and eastern parts of the Tibetan Plateau, in the East Kunlun and Qilian Shan (e.g. Liu et al., 2017; Qi et al., 2016), and west Longmenshan (e.g. Roger et al., 2011), as well as in the Pamir (e.g. Cao et al., 2013) and western Tianshan further north (e.g. De Gravé et al., 2013; Dumitru et al., 2001) (Fig. 9). Our new data add to this regional picture in also confirming a record of cooling throughout the West Kunlun.

We hypothesise that the Jurassic pause in cooling (Figs. 4 and 6) reflects the persistence of the elevated topography along the (southern) West Kunlun-Songpan-Ganzi and northern Tianshuihai, accompanying continuous northward subduction of the Meso-Tethys oceanic slab (e.g. Yin and Harrison, 2000). The lack of Jurassic marine sediments within the West Kunlun, Songpan-Ganzi, and northern Tianshuihai contrasts with thick Jurassic terrestrial deposits in the southern Tianshuihai terrane (Mattern and Schneider, 2000), which were likely derived from the southern margin of the paleo-plateau (e.g. Songpan-Ganzi, northern Tianshuihai terranes). While this is similar to that reported from the northeastern Tibetan Plateau (e.g. Roger et al., 2011; Tian et al., 2014;

Liu et al., 2017, and references therein; Fig. 9), further investigations will be required to test this hypothesis.

We associate the pronounced Early Cretaceous cooling/exhumation episode in the West Kunlun with collision between the Karakorum-Taishuihai terranes and Lhasa terrane along the Bangong-Nujiang suture (closure of the Meso-Tethys Ocean; e.g. Yin and Harrison, 2000 and references therein). This is supported by evidence for slip on several major regional faults system at this time, e.g. Tam Karaul fault (Cowgill, 2001), Karakax fault (Arnaud et al., 2003), and a south-verging backthrust in the Tianshuihai terrane (Cowgill, 2001), perhaps as well as the Kashgar-Yecheng transfer system (Yin et al., 2002). This exhumation episode is recorded by low temperature thermochronology data with a slight variation in timing throughout the northern and eastern Tibetan Plateau (e.g. East Kunlun, Qilian Shan, Longmen Shan), the Pamir and the Tianshan (also see Fig. 9), consistent with significant Early Cretaceous crustal shortening and thickening throughout Tibet and Pamir, as well as the Tianshan (e.g. Yin, 2006; Kapp et al., 2007; De Gravé et al., 2013; Tian et al., 2014; Robinson, 2015).

The localized nature of the relative rapid Late Cretaceous cooling in samples (WK17-42~45; Fig. 4) in the immediate hanging walls of the Tam Karaul and Tiklik faults (Fig. 4), probably reflects the restricted thermal impact of fault motion. We note that this was coeval with collision between the Karakorum terrane and Kohistan-Ladakh Arc (Rehman et al., 2011), located directly to the south (Fig. 1A). Late Cretaceous cooling is also recorded in the north and central Tibetan Plateau and Tianshan regions, where it was accompanied by reactivation of the regional/local fault systems (Tian et al., 2014; Liu et al., 2017; see Fig. 9).

The Paleocene-Early Eocene rapid cooling/exhumation is limited to samples in close proximity to and on the north side of the Karakax strike-slip fault. This suggests rather localized fault reactivation coincident with initial India-Asia collision between ~65–52 Ma (e.g. Hu et al., 2016, and references therein). It is notable that only a few scattered cooling events of this age have been reported from the Tibet-Tianshan region (see Fig. 9) and we propose that this can probably be attributed to the relatively limited response in the West Kunlun and surrounding regions to the initial India-Asia collision.

Similarly, two samples from close to the Karakax and Tiklik faults (Fig. 3) show relatively fast cooling/exhumation commencing in the Middle Eocene, consistent with results reported by Cowgill (2001) (Figs. 2, 4), which we attribute to fault reactivation at that time. All other samples show relatively subdued Middle Eocene-Early Oligocene activity, consistent with the relative quiescence noted in the Songpan-Ganzi, Qiangtang and Lhasa terranes.

Foreland basin deposition in the southwestern Tarim Basin initiated in the Eocene, but developed more broadly in the Oligocene (e.g. Jiang and Li, 2014; Blayney et al., 2016), which is coeval with denudation and cooling of the northern sub-terrane of the West Kunlun due to exhumation along the Tiklik fault. This has been considered to reflect plateau expansion outwards to the Lhasa terrane, accompanied by regional magmatism and crustal thickening (e.g. Kapp et al., 2007). Regionally, thermochronology data summarized in Fig. 9 have revealed several exhumation events commencing in the Middle Eocene, which are also linked to reactivation of regional/local fault systems (Yin, 2006) presumably in response to ongoing shortening along the West Kunlun range front that accommodates a small proportion of the ongoing India-Asia convergence following collision.

As with previous studies, our thermal history modeling reveals a prominent latest Oligocene-Miocene cooling of widespread exhumation, through the AFT partial annealing zone (120–60 °C in Fig. 4 and supporting information). This episode is well-documented across the entire West Kunlun range (Cao et al., 2015;

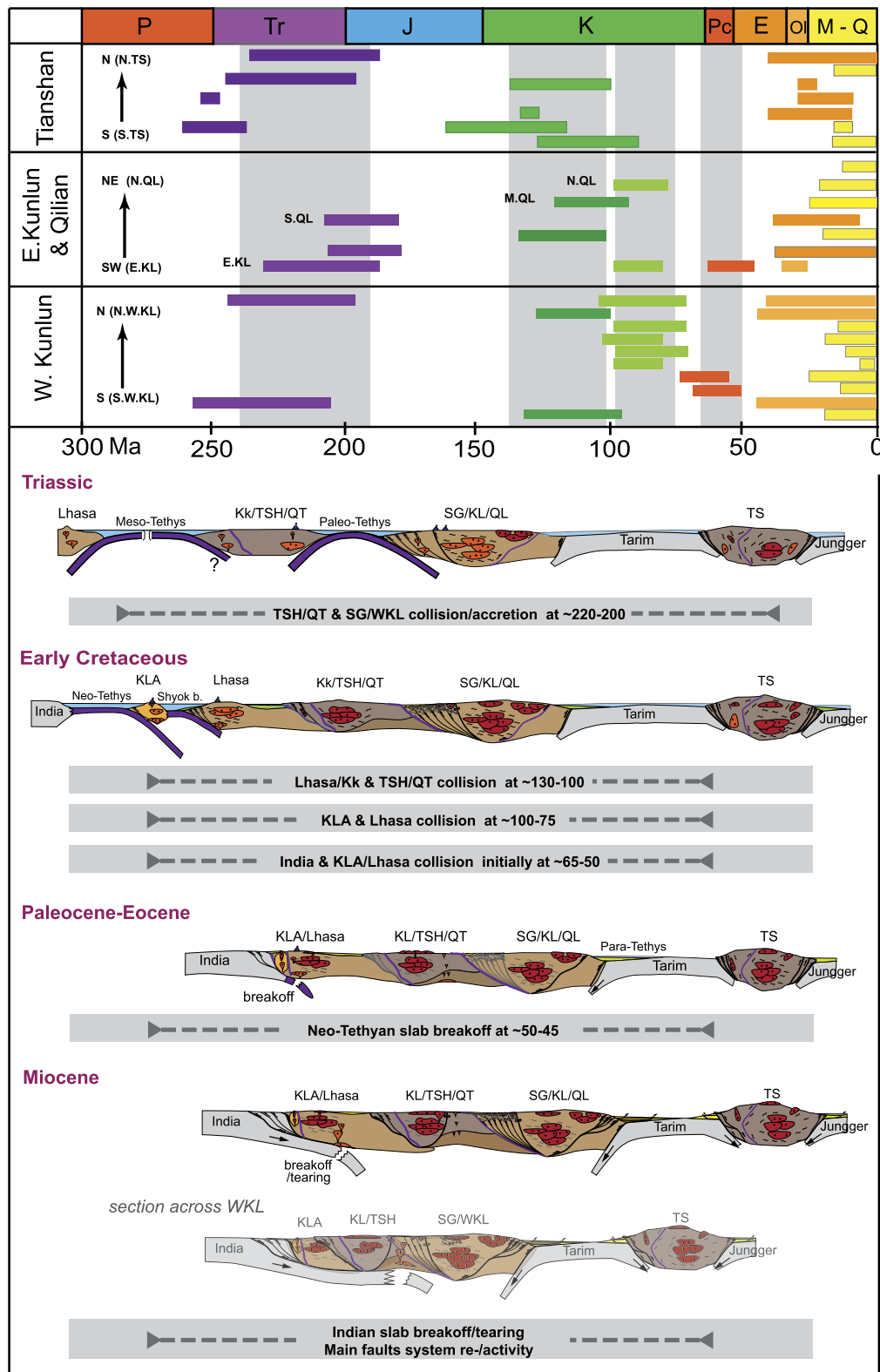


Fig. 9. Upper panel: Summary showing fast cooling episodes along the northern margin of the Tibetan Plateau (West Kunlun, East Kunlun and Qilian Shan) and Tianshan orogenic belt. Cooling episodes from thermal history modeling of the Tianshan after Dumitru et al. (2001), De Grave et al. (2013) and references therein; Longmenshan: Roger et al. (2011), Wang et al. (2012), Tian et al. (2014); and East Kunlun and Qilianshan: Liu et al. (2017), Qi et al. (2016). West Kunlun: Cowgill (2001), Chen et al. (2017) and this study. Lower panel: tectonic evolution of the Tibetan Plateau and the Tianshan orogenic belt, modified after Yin and Harrison (2000), Rehman et al. (2011) and Cao et al. (2015). KL – Kunlun; QL – Qilian; QT – Qiangtang; SG – Songpan-Ganzi; TS – Tianshan.

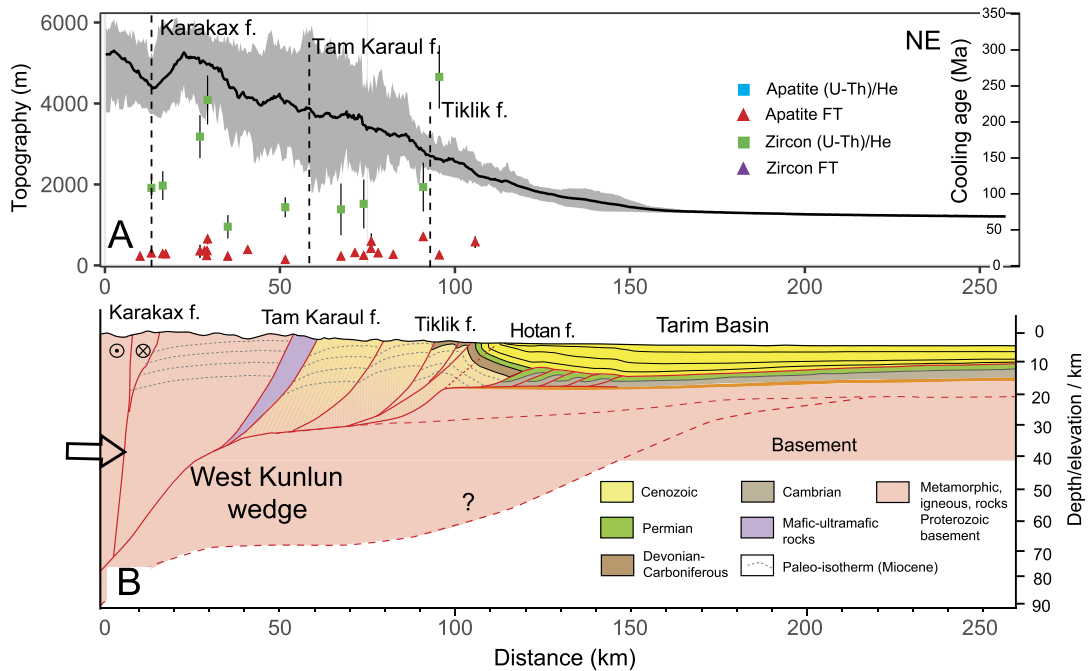


Fig. 10. North-south distribution of cooling ages (A) and north-south structural cross sections (B, modified from Guilbaud et al., 2017) along the West Kunlun via Yecheng. Mean topographic profile for the transect (A) is represented by the bold black line and minimum/maximum elevations by the thin black lines.

Jiang and Li, 2014; Wang et al., 2003; and references therein), and accompanied reactivation of all the major fault systems (e.g. Tiklik, Tam Karaul, Karakax faults, KYTS, Hotan thrust; e.g. Sobel and Dumitru, 1997; Arnaud et al., 2003; Wang et al., 2003; Yin et al., 2002; Fig. 10). The appearance of coeval coarse sediments (e.g. Cao et al., 2015; Zheng et al., 2015) and propagation of frontal thrusts (e.g. Jiang and Li, 2014; Zheng et al., 2015) in the Tarim foreland, all signal renewed plateau expansion along the entire West Kunlun at this time. It is notable that this timing corresponds broadly with significant reorganization within other orogenic systems that bound Tibet such as the Himalaya, which is linked to development of the Siwalik foreland basin and associated activity of the Main Central, Main Boundary and Main Frontal thrusts (Yin, 2006; and references therein). Neogene cooling is prevalent throughout all margins of the Tibetan Plateau and Tianshan region (e.g. De Grave et al., 2013; Yin and Harrison, 2000; Yin, 2006; Fig. 9), and marks a major rejuvenation of the present Tibetan Plateau, with shortening across the entire plateau, possibly accompanied by mantle lithosphere removal (Molnar et al., 2010 and references therein).

As described above, our thermochronology data from the West Kunlun shows a large age spread (AFT: ~7–40 Ma and ZHe: ~47–265 Ma), contrasting with the Himalaya, where cooling ages tend to be much younger (typically <12 Ma) with a much narrow spread in ages. Given fundamental differences in convergence rates and climate between the two margins, such differences are hardly surprising. The modern convergence rate across the West Kunlun is approximately 5 km/myr (Guilbaud et al., 2017; references therein). Assuming that the entire 100 km width of the orogenic front from the Karakax fault to the Tarim foreland (Fig. 10) is eroding at about 0.2 km/myr, then erosion accounts for only about 10% of the crustal convergence. In general, our new results are entirely consistent with a slowly accreting, relatively arid, intracontinental mountain belt, in which the role of orogenic thermal advection is greatly subdued, comparable to ancient low thermal Peclet number intraplate orogens (e.g. Sandiford, 2002).

Receiver function studies cited by Craig et al. (2012) show that at 90 km the crust beneath the Karakax fault system in the West

Kunlun is the thickest in the entire Tibetan plateau. Significantly, because the deepest part of this crust appears to be seismically active, it must also be relatively cool (Craig et al., 2012). The nature and origin of the ~90 km thick crust to the south of the Karakax (Fig. 10B) remains more obscure. Craig et al. (2012) have postulated that the deep crustal earthquakes in this region map the northern extent of Indian continental crust underthrust beneath the Tibetan plateau (see also McKenzie et al., 2019). In this scheme, the underthrust Indian crust and Tarim crust are likely juxtaposed along the Karakax fault, and it seems plausible that the initiation of the Karakax fault coincides with, or closely follows from, this juxtaposition. Similar arguments have been made for the Pamir, where intermediate depth mantle seismicity has been interpreted as reflecting ongoing subduction presumed to have initiated at around 12 Ma, possibly associated with consumption of the relic former ocean lithosphere (McKenzie et al., 2019). In the West Kunlun, we surmise that it is the interaction of the thick, relatively cold and deeply seismogenic crust to the south of the Karakax fault with the Tarim crust that results in the partitioning of deformation between relatively limited crustal shortening in the foreland and strike slip faulting on the Karakax fault. We note that the imprint of accelerated late Neogene cooling in all samples analyzed here coincides with the putative onset of fast slip on the Karakax fault.

In more general terms, the new results presented here are consistent with the notion that the West Kunlun in an intraplate system formed as a consequence, and continuing to be driven by, in plane forces transmitted through the surface plates. An obvious source of stress is the gravitational potential energy (i.e. the buoyancy force) arising from ongoing plateau construction, which itself is attributable to the plate wide system of force balance that sustains Indian-Asian collision. Further, we suggest that it is the communication facilitated via in-plane transmission of stress that provides the principal mechanism for synchronizing the thermochronological record between the distant orogenic systems that bound the Tibetan plateau, as further evidenced by the general correlations evident in the new thermochronological dataset presented here.

7. Conclusion

New thermochronology results from the West Kunlun, a long-lived orogenic belt, records multiple cooling events accompanying a series of Phanerozoic accretion/collision events. Different cooling/exhumation scenarios of varying intensity can be discerned, accompanied by episodic activity of regional fault systems (e.g. Tiklik, Tam Karaul, Karakax faults, KYTS). These episodes are all considered to mark orogenic events along the southern Asian margin, e.g. between the West Kunlun, Songpan-Ganzi and Tianshuihai terranes [Late Permo-Triassic], the Qiangtang and Lhasa terranes [Early Cretaceous], the Karakorum terrane and Kohistan-Ladakh Arc [Late Cretaceous] and India and Asia [ongoing since the Paleocene]. These cooling episodes are also comparable with those of the northern and eastern margins of the Tibetan Plateau and Tianshan region. Further, compared with the Himalaya, the preservation of a long-lived exhumation history of the West Kunlun revealed by low temperature thermochronology data can mainly be attributed to a slow regional convergence and low erosion rates.

Acknowledgements

Funding for this research was provided by Australia Research Council Discovery Early Career Research Award (DECRA, DE120102245), IGGCAS Open Research Foundation (SKL-K201702) and NSFC (No. 41562007). The University of Melbourne thermochronology laboratory receives infrastructure support under the AuScope Program of the National Collaborative Research Infrastructure Strategy (NCRIS). We are grateful to Abaz Alimanovic for assistance with ZHe dating. We thank Ed Sobel and an anonymous reviewer for their very constructive comments on earlier versions of this work and An Yin for editorial handling.

Appendix A. Supplementary material

Supplementary material related to this article can be found online at <https://doi.org/10.1016/j.epsl.2019.115833>.

References

- Arnaud, N., Tapponnier, P., Roger, F., Brunel, M., Scharer, U., Wen, C., Zhiqin, X., 2003. Evidence for Mesozoic shear along the western Kunlun and Altyn-Tagh fault, northern Tibet (China). *J. Geophys. Res.* 108, 2053. <https://doi.org/10.1029/2001JB000904>.
- Blayney, T., Najman, Y., Dupont-Nivet, G., Carter, A., Millar, I., Garzanti, E., Sobel, E.R., Rittner, M., Andò, S., Guo, Z., Vezzoli, G., 2016. Indentation of the Pamirs with respect to the northern margin of Tibet: constraints from the Tarim basin sedimentary record. *Tectonics* 35, 2345–2369. <https://doi.org/10.1029/2016TC004222>.
- Cao, K., Wang, G.C., Bernet, M., van der Beek, P., Zhang, K.X., 2015. Exhumation history of the West Kunlun Mountains, northwestern Tibet: evidence for a long-lived, rejuvenated orogen. *Earth Planet. Sci. Lett.* 432, 391–403.
- Cao, K., Wang, G.C., van der Beek, P., Bernet, M., Zhang, K.X., 2013. Cenozoic thermos-tectonic evolution of the northeastern Pamir revealed by zircon and apatite fission-track thermochronology. *Tectonophysics* 589, 17–32.
- Cao, K., Xu, Y.D., Wang, G.C., Zhang, K.X., van der Beek, P., Wang, C.W., Jiang, S.S., John Bershaw, J., 2014. *J. Geol.* 122 (4), 433–454.
- Cheng, X.G., Chen, H.L., Lin, X.B., Wu, L., Gong, J.F., 2017. Geometry and kinematic evolution of the Hotan-Tiklik segment of the Western Kunlun Thrust Belt: constrained by structural analyses and Apatite Fission Track thermochronology. *J. Geol.* 125, 65–82.
- Clark, M.K., Farley, K.A., Zheng, D., Wang, Z., Duvall, A.R., 2010. Early Cenozoic faulting of the northern Tibetan Plateau margin from apatite (U-Th)/He ages. *Earth Planet. Sci. Lett.* 296 (1), 78–88.
- Cowgill, E., 2001. Tectonic Evolution of the Altyn Tagh-Western Kunlun Fault System, Northwestern China. Ph.D. thesis. University of California Los Angeles.
- Craig, T.J., Johnson, A., Jackson, J., 2012. Thermal and tectonic consequences of India underthrusting Tibet. *Earth Planet. Sci. Lett.* 353–354, 231–239. <https://doi.org/10.1016/j.epsl.2012.07.010>.
- De Grave, J., Glorie, S., Buslov, M.M., Stockli, D.F., McWilliams, M.O., Batalev, V.Y., van den Haute, P., 2013. Thermo-tectonic history of the Issyk-Kul basement (Kyrgyz Northern Tien Shan, Central Asia). *Gondwana Res.* 23 (3), 998–1020. <https://doi.org/10.1016/j.gr.2012.06.014>.
- Ding, L., Kapp, P., Wan, X., 2005. Paleocene-Eocene record of ophiolite obduction and initial India-Asian collision, south central Tibet. *Tectonics* 24 (3). <https://doi.org/10.1029/2004TC001729>. TC3001.
- Dumitru, T.A., Zhou, D., Chang, E.Z., Graham, S.A., Hendrix, M.S., Sobel, E.R., Carroll, A.R., 2001. Uplift, exhumation, and deformation in the Chinese TianShan. *Mem. Geol. Soc. Am.*, 71–100.
- Farley, K.A., Wolf, R.A., Silver, L.T., 1996. The effects of long alpha-stopping distances on (U-Th)/He ages. *Geochim. Cosmochim. Acta* 60, 4223–4229.
- Fitzgerald, P.G., Malusà, M.G., 2019. Concept of the exhumed partial annealing (retention) zone and age-elevation profiles in thermochronology. In: Malusà, M.G., Fitzgerald, P.G. (Eds.), *Fission-Track Thermochronology and Its Application to Geology*. Springer, pp. 165–189.
- Fu, B.H., Zhang, S.L., Xie, X.P., Shi, X., Wang, S., 2006. Late quaternary tectono-geomorphic features along the Kangxiwar fault, Altyn Tagh fault system, Northern Tibet. *Quat. Sci.* 26, 228–235.
- Gleadow, A., Harrison, M., Kohn, B., Lugo-Zazueta, R., Phillips, D., 2015. The Fish Canyon Tuff: a new look at an old low-temperature thermochronology standard. *Earth Planet. Sci. Lett.* 424, 95–108.
- Guenther, W.R., Reiners, P.W., Ketcham, R.A., Nasdala, L., Giester, G., 2013. Helium diffusion in natural zircon: radiation damage, anisotropy, and the interpretation of zircon (U-Th)/He thermochronology. *Am. J. Sci.* 313 (3), 145–198.
- Guilbaud, C., Simoes, M., Barrier, L., Laborde, A., Van der Woerd, J., Li, H., Murray, A., 2017. Kinematics of active deformation across the Western Kunlun mountain range (Xinjiang, China) and potential seismic hazards within the southern Tarim Basin. *J. Geophys. Res., Solid Earth* 122, 10,398–10,426.
- Hu, X., Garzanti, E., Wang, J., Huang, W., An, W., Alex, Webb, 2016. The timing of India-Asia collision onset – facts, theories, controversies. *Earth-Sci. Rev.* 160, 264–299.
- Jiang, X., Li, Z., 2014. Seismic reflection data support episodic and simultaneous growth of the Tibetan Plateau since 25 Myr. *Nat. Commun.* 5, 1–7.
- Kapp, P., DeCelles, P.G., Gehrels, G.E., Heizler, M., Ding, L., 2007. Geological records of the Lhasa-Qiangtang and Indo-Asian collisions in the Nima area of central Tibet. *Geol. Soc. Am. Bull.* 119 (7–8), 917–933.
- Ketcham, R.A., Carter, A., Donelick, R.A., Barbarand, J., Hurford, A.J., 2007. Improved modeling of fission-track annealing in apatite. *Am. Mineral.* 92 (5–6), 799–810.
- Lacassin, R., Valli, F., Arnaud, N., Leloup, P.H., Paquette, J.L., Haibing, L., et al., 2004. Large-scale geometry, offset and kinematic evolution of the Karakorum fault, Tibet. *Earth Planet. Sci. Lett.* 219, 255–269.
- Li, Y., Wang, C., Dai, J., Xu, G., Hou, Y., Li, X., 2015. Propagation of the deformation and growth of the Tibetan-Himalayan orogen: a review. *Earth-Sci. Rev.* 143, 36–61.
- Liu, D., Li, H., Sun, Z., Pan, J., Wang, M., Wang, H., Marie, L., 2017. AFT dating constrains the Cenozoic uplift of the Qimen Tagh Mountains, Northeast Tibetan Plateau, comparison with LA-ICPMS Zircon U-Pb ages. *Gondwana Res.* 41, 438–450.
- Mancktelow, N.S., Grasemann, B., 1997. Time-dependent effects of heat advection and topography on cooling histories during erosion. *Tectonophysics* 270, 167–195.
- Mattern, F., Schneider, W., 2000. Suturing of the Proto- and Paleo-Tethys oceans in the western Kunlun (Xinjiang, China). *J. Asian Earth Sci.* 18 (6), 637–650.
- McKenzie, D.P., Jackson, J.A., Priestley, K.F., 2019. Continental collisions and the origin of subcrustal continental earthquakes. *Can. J. Earth Sci.* <https://doi.org/10.1139/cjes-2018-0289> (in press).
- Molnar, P., Boos, W.R., Battisti, D.S., 2010. Orographic controls on climate and paleoclimate of Asia: thermal and mechanical roles for the Tibetan Plateau. *Annu. Rev. Earth Planet. Sci.* 38 (1), 77–102.
- Qi, B., Hu, D., Yang, X., Zhang, Y., Tan, C., Zhang, P., Feng, C., 2016. Apatite fission track evidence for the Cretaceous-Cenozoic cooling history of the Qilian Shan (NW China) and for stepwise northeastward growth of the northeastern Tibetan Plateau since early Eocene. *J. Asian Earth Sci.* 124, 28–41.
- Rehman, H.U., Seno, T., Yamamoto, H., Khan, T., 2011. Timing of collision of the Kohistan-Ladakh Arc with India and Asia: debate. *Isl. Arc* 20 (3), 308–328.
- Robinson, A.C., 2015. Mesozoic tectonics of the Gondwanan terranes of the Pamir plateau. *J. Asian Earth Sci.* 102, 170–179.
- Roger, F., Jolivet, M., Cattin, R., Malavieille, J., 2011. Mesozoic-Cenozoic tectonothermal evolution of the eastern part of the Tibetan Plateau (Songpan-Garzé, Longmen Shan area): insights from thermochronological data and simple thermal modelling. *Geol. Soc. (Lond.) Spec. Publ.* 353 (1), 9–25.
- Sandiford, M., 2002. Low thermal Pelet number intraplate orogeny in central Australia. *Earth Planet. Sci. Lett.* 201, 309–320.
- Sobel, E.R., Dumitru, T.A., 1997. Thrusting and exhumation around the margins of the western Tarim basin during the India-Asia collision. *J. Geophys. Res.* 102, 5043–5063.
- Tapponnier, P., Xu, Z., Roger, F., Meyer, B., Arnaud, N., Wittlinger, G., Yang, J., 2001. Oblique stepwise rise and growth of the Tibet Plateau. *Science* 294, 1671–1677.
- Thiede, R.C., Ehlers, T.A., 2013. Large spatial and temporal variations in Himalayan denudation. *Earth Planet. Sci. Lett.* 371–372, 278–293.
- Tian, Y., Kohn, B.P., Gleadow, A.J.W., Hu, S., 2014. A thermochronological perspective on the morphotectonic evolution of the southeastern Tibetan Plateau. *J. Geophys. Res., Solid Earth* 119 (1), 676–698. <https://doi.org/10.1002/2013jb010429>.

- Wang, E., Kirby, E., Furlong, K.P., Soest, M.V., Xu, G., Shi, X., Hodges, K.V., 2012. Two-phase growth of high topography in eastern Tibet during the Cenozoic. *Nat. Geosci.* <https://doi.org/10.1038/Ngeo1538>.
- Wang, Erchie, Wan, J., Liu, Jiaqi, 2003. Late Cenozoic geological evolution of the foreland basin bordering the West Kunlun range in Pulu area: constraints on timing of uplift of northern margin of the Tibetan Plateau. *J. Geophys. Res.* 108 (B8), 2401. <https://doi.org/10.1029/2002JB001877>.
- Wang, J., Wang, S.Y., Zhang, Q.H., Cui, J.T., Luo, Q.Z., Peng, S.M., Liu, C.L., 2004. Reports of Geological Survey Mapping for Yechang and Kangxiwa Areas, 1:250000. *Geological Survey of China*, 880 pp. (in Chinese).
- Wei, W., Zhou, Z., 2009. Reconstruction of palaeotopography from low-temperature thermochronological data. *Geol. Soc. (Lond.) Spec. Publ.* 324, 99–110. <https://doi.org/10.1144/SP324.8>.
- Xiao, W., Han, F., Windley, B.F., Yuan, C., Zhou, H., Li, J., 2003. Multiple accretionary orogenesis and episodic growth of continents: insights from the Western Kunlun Range, Central Asia. *Int. Geol. Rev.* 45 (4), 303–328.
- Xiao, F., Windley, B.F., Sun, S., 2015. A tale of amalgamation of three Permo-Triassic collage systems in central Asia: oroclines, sutures, and terminal accretion. *Annu. Rev. Earth Planet. Sci.* 43, 477–507.
- Yin, A., 2006. Cenozoic tectonic evolution of the Himalayan orogen as constrained by along strike variation of structural geometry, exhumation history, and foreland sedimentation. *Earth-Sci. Rev.* 76, 1–131.
- Yin, A., Harrison, T.M., 2000. Geologic evolution of the Himalayan–Tibetan orogen. *Annu. Rev. Earth Planet. Sci.* 28, 211–280.
- Yin, A., Rumblehart, P.E., Butler, R., Cowgill, E., Harrison, T.M., Foster, D.A., Ingwersen, R.V., Qing, Z., Xian-Qiang, Z., Xiao-Feng, W., Hanson, A., Raza, A., 2002. Tectonic history of the Altyn Tagh fault system in northern Tibet inferred from Cenozoic sedimentation. *Geol. Soc. Am. Bull.* 114, 1257–1295.
- Zhang, P., Shen, Z., Burgman, R., Molnar, P., Wang, Q., Niu, Z., Sun, J., Wu, J., Sun, H., You, X., 2004. Continuous deformation of the Tibetan Plateau constrained from global positioning measurements. *Geology* 32 (9), 809–812.
- Zhao, G., Cawood, P.A., 2012. Precambrian geology of China. *Precambrian Res.* 222–223, 13–54.
- Zheng, H., Wei, X., Tada, R., Clift, P.D., Wang, B., Jourdan, F., Wang, P., He, M., 2015. Late Oligocene–early Miocene birth of the Taklimakan Desert. *Proc. Natl. Acad. Sci. USA* 112 (25), 7662–7667.